

MAXIMUM ENERGIES OF FORCE-FREE CORONAL FLUX ROPES

RICHARD WOLFSON AND JONATHAN LARSON

Department of Physics, Middlebury College, Middlebury, VT 05753; wolfson@middlebury.edu, jonathan.larson@bos.frb.org

AND

ROBERTO LIONELLO

Science Applications International Corporation, San Diego, CA 92121; lionellor@saic.com

Received 2006 September 15; accepted 2007 January 29

ABSTRACT

Magnetic energy is believed to play a major role in powering coronal mass ejections (CMEs). Free magnetic energy is associated with electric currents that give the magnetic field more energy than a purely potential (current-free) field. For magnetic energy alone to power a CME, the energy must be sufficient to open the magnetic field to interplanetary space, to lift the ejecta against solar gravity, and to accelerate the ejecta. However, the coronal magnetic field is very nearly force free, and force-free fields attached to the coronal base cannot contain more energy than that of the fully open field with the same boundary conditions. We therefore explore force-free fields containing detached magnetic flux ropes, with the goal of finding the maximum possible energy stored in such configurations. We use a maximizing algorithm that searches a space of four parameters to find the maximum energy solution. Our results show a broad maximum in parameter space, with energies in excess of the open-field energy by about 18% of the corresponding potential-field energy. Confinement of nonpotential fields close to the solar equator enhances the energy storage, with maximum energies generally corresponding to more extreme confinement. This suggests that overlying potential fields can hold down a nonpotential field, allowing substantial energy buildup.

Subject headings: MHD — Sun: corona — Sun: magnetic fields

1. INTRODUCTION

Coronal mass ejections (CMEs) typically expel some 5×10^{15} g of coronal material into interplanetary space at speeds of several hundred km s^{-1} . The energy involved, some 10^{32} erg, is needed not only to accelerate the ejecta to such speeds, but also to lift the material against solar gravity, and most significantly, to open the coronal magnetic field for solar plasma to escape into interplanetary space. A theorem by Aly (1984, 1991) and Sturrock (1991) suggests that the energy of a fully open field is an upper limit on the energies of force-free fields in simple geometries. Therefore, simple force-free fields cannot store sufficient energy for all three CME tasks. However, more complex force-free fields, in particular those containing detached magnetic flux, are not subject to the Aly-Sturrock limit. Earlier work with detached flux has produced force-free configurations with energies beyond the Aly limit, but in most cases barely so, with the excess only a few percent of the corresponding potential-field energy (Wolfson 2003; Flyer et al. 2004). One flux rope study using a low- β MHD simulation did somewhat better, producing nearly force-free fields with excess energy of some 11% of the potential-field energy (Li & Hu 2003). More complex topologies with embedded current sheets can do still better, exceeding the open-field energy by some 36% of the potential-field energy (Choe & Cheng 2002).

This paper explores the energetics of detached force-free magnetic flux ropes in an axisymmetric model corona. We search systematically through a space of four parameters that characterize the magnetic field in terms of its flux distribution at the coronal base and the amount and distribution of azimuthal flux. The latter, generally associated with shearing of the magnetic footpoints, is what gives rise to field-aligned currents and correspondingly to magnetic energy in excess of the potential-field energy.

2. CHARACTERIZING MAGNETIC ENERGIES

We consider four distinct energies that characterize magnetic fields with a given distribution of magnetic flux at the coronal base. Lowest is the energy U_{pot} of the unique potential field that is strictly poloidal and current free in the infinite domain beyond the coronal base. Throughout this paper we will use U_{pot} as a reference energy, normalizing all other energies to its value. This is not a trivial point, because we consider different distributions of magnetic flux at the coronal base, and these have different values of U_{pot} for the same radial magnetic field at a given latitude at the coronal base. Therefore, the decision to normalize using U_{pot} means letting the actual radial base field vary so that the energy of potential fields with different base flux distributions remains the same. A second characteristic energy is U_{open} , the energy of the fully open field with the same base flux distribution. We consider only configurations with symmetry about the equator, and in such cases the fully open field is current free except for a current sheet in the equatorial plane, separating regions of oppositely directed field. A third characteristic energy is the energy U of an arbitrary force-free field, generally containing volume currents and an azimuthal field component and again having the same base flux distribution. The energy U can be computed as a volume integral of the magnetic energy density, or as a surface integral using the scalar virial theorem (see Priest 1984), which relates surface and volume integral contributions to the magnetic energy contained in a plasma. For a force-free magnetic field in axisymmetric spherical geometry, the virial theorem takes the form (Wolfson & Low 1992)

$$U = \int \int \int (B_r^2 + B_\theta^2 + B_\phi^2) d\tau = \int \int (B_r^2 - B_\theta^2 - B_\phi^2) d\sigma. \quad (1)$$

Here $d\tau$ and $d\sigma$ are the volume and surface area elements, respectively, and \mathbf{B} is the magnetic field, expressed here in spherical polar coordinates. The left-hand integral is taken over the infinite volume above the coronal base, while the surface integral on the right is over the base alone (more generally, the surface integral involves all bounding surfaces, but here the outer boundary is at infinity and makes no contribution). Both integrals give U , the magnetic energy, in the same arbitrary units. The existence of two distinct expressions for U provides a check on numerical solutions. In the work described here, the two always agree to better than 1 part in 10^3 , and in most cases to better than 1 part in 10^5 . Because the virial theorem holds for force-free fields only, this provides an excellent check that the solutions are indeed force free. A final characteristic energy also follows from the virial theorem. The virial surface integral shows that the absolute maximum energy, U_{\max} , is given by taking the surface integral with $B_\theta = B_\phi = 0$, and thus integrating only B_r^2 . Such a field is strictly radial at the coronal base and is generally not force free. However, it represents an absolute upper limit on the possible magnetic energy associated with a given flux distribution at the coronal base.

3. PARAMETER SPACE

For a given solution, the difference $U_{\text{free}} = U - U_{\text{pot}}$ represents the free energy that could be released through the dissipation or other collapse of the force-free currents, and this is the energy that is, in principle, available to power a mass ejection. However, the energy $U_{\text{open}} - U_{\text{pot}}$ is required to open the field, and therefore the energy available to lift and propel the ejecta is the smaller quantity $U_{\text{excess}} = U - U_{\text{open}}$. Therefore, our goal is to find force-free magnetic flux rope solutions with the maximum excess energy U_{excess} ; that is, solutions whose energy U exceeds the open-field energy U_{open} by the maximum possible amount. Again, we express all energies in units of the appropriate energy U_{pot} .

We work in axisymmetric spherical geometry, and parameterize our solutions with the four parameters described below.

First is the parameter α , which characterizes the magnetic flux distribution at the coronal base, as described in Wolfson (2003). Our solutions are given in terms of a flux function $\psi(r, \theta)$, which in our axisymmetric spherical geometry is $\psi = A_\phi r \sin \theta$, with A being the magnetic vector potential. The boundary condition at the coronal base is specified by giving $\psi(1, \theta)$, which we take to be

$$\psi(\mu) = \psi_0(1 - |\mu|^\alpha), \quad (2)$$

where $\mu = \cos \theta$ and ψ_0 is a parameter that sets the overall scale of the magnetic field. In this work we choose $\psi_0 = 1$, which gives the base magnetic field at the equator the dimensionless value of 1. The important parameter is α , which determines the distribution of magnetic flux at the coronal base. The case $\alpha = 2$ makes the potential field that of a pure dipole, with $B_r \propto \mu$ at the coronal base. More generally, the base radial field is

$$B_r(r = 1) = \pm \psi_0 \alpha |\mu|^{\alpha-1}, \quad (3)$$

where the positive and negative signs indicate the northern and southern hemispheres, respectively. Thus, higher values of alpha correspond to fields in which the base flux is distributed more toward the poles.

The second parameter is a cutoff latitude, designated L^* , beyond which the field at the coronal base is current free. Thus, any magnetic shear at the coronal base is confined to latitudes equatorward of L^* . The choice of L^* and the base flux distribution parameter α together determine a value ψ^* for the field line that

separates potential from nonpotential fields. Decreasing L^* decreases the magnetic flux emerging from the coronal base in the nonpotential field, and may or may not change the volume occupied by a sheared, nonpotential field depending on the shape of the field line with $\psi = \psi^*$. Physically, a decrease in L^* results in more overlying potential field, which should enhance any ‘‘hold down’’ effect in which the potential field keeps the sheared field from erupting outward.

The third and fourth parameters relate to the form of the magnetic shear, or more directly, to the azimuthal magnetic field. We solve for the flux function ψ using the well-known Grad-Shafranov equation, which in axisymmetric spherical coordinates takes the form (see Wolfson 1995)

$$\frac{\partial^2 \psi}{\partial r^2} + \frac{1 - \mu^2}{r^2} \frac{\partial^2 \psi}{\partial \mu^2} = -f \frac{df}{d\psi}, \quad (4)$$

where $\mu = \cos \theta$. Here f is an arbitrary function of the flux function ψ , related to the azimuthal field component by

$$B_\phi = \frac{f(\psi)}{r \sin \theta}, \quad (5)$$

and indirectly to the magnetic shear via integration over the field lines determined from the solution.

The remaining parameters involve the function f , which we take to have the form

$$f(\psi) = \begin{cases} \gamma \left(\frac{\psi - \psi^*}{\psi_0 - \psi^*} \right)^\beta & \psi > \psi^*, \\ 0 & \psi \leq \psi^*, \end{cases} \quad (6)$$

where ψ_0 and ψ^* were defined earlier. The third parameter for our parameter-space exploration is β , which determines the shape of the function f ; lower values of β spread the shear over the entire region between the equator and L^* , while higher values tend to concentrate shear more toward the equator. For the case $L^* = 90^\circ$, allowing the nonpotential field to extend to infinity, our β is related to the parameter n of Flyer et al. (2004, hereafter FL04) by

$$n = 2\beta - 1. \quad (7)$$

The parameter γ is a scaling factor that describes the size of the nonlinear source term in equation (4). It is related, but not necessarily monotonically, to the overall deviation from potential field, and thus to the azimuthal field strength and the magnetic footpoint shear; $\gamma = 0$ corresponds to the potential field. Our γ relates to a similarly named parameter used in FL04, and here designated γ_{FL} , by

$$\gamma_{\text{FL}} = \beta \gamma^2. \quad (8)$$

However, γ is *not* our fourth parameter. This is because (1) γ itself is not particularly meaningful physically (Low 1977; Klimchuk & Sturrock 1989), and (2) solution sequences produced by increasing γ monotonically end at critical points beyond which γ decreases as the solution sequence proceeds along a new branch. Together, these issues make γ less than the ideal parameter for characterizing solutions to equation (4). Instead, FL04 have suggested characterizing similar force-free solutions by the total azimuthal magnetic flux F_ϕ , obtained by integrating $B_\phi = f(\psi)/r \sin \theta$ over the r - θ plane. This characterization is

appropriate because the azimuthal flux increases monotonically along a solution sequence.

Thus, we have four distinct parameters that characterize a given solution. The first, α , determines the distribution of magnetic flux at the coronal base; higher α values correspond to greater poleward flux concentration. The second, L^* , is the cutoff latitude, above which field lines at the coronal base are not sheared, and the field is therefore potential. The third parameter is β , which determines the shape of the generating function; lower β values spread shear and currents more evenly across the region of nonpotential field. The fourth parameter, F_ϕ , is the azimuthal magnetic flux.

Strictly speaking, our results are valid only in the context of the generating function specified in equation (6), so it might be possible to find higher maximum energies with other forms of this function. However, our use of four free parameters ensures that equation (6) actually describes a broad range of possible generating functions. The shape parameter β , in particular, lets the function $f(\psi)$ vary from extremes of upward concavity to downward concavity, and thus it represents the general features of all inflection-free monotonic functions. Therefore, our results are likely to give a close approximation to the maximum energies attainable in simple arcade-like magnetic fields.

4. COMPUTATIONAL APPROACH

Specification of these four parameters determines a solution to the nonlinear partial differential equation (4), should such a solution exist. But that equation contains γ rather than the azimuthal flux F_ϕ , and because F_ϕ is an integral involving $f(\psi)$, with ψ the solution, it might seem that F_ϕ cannot be prescribed a priori. We get around this problem by adding another degree of freedom to the system that results from discretizing equation (4), in the form of a weak constraint that reads

$$\gamma(F_t - F_\phi) = 0. \quad (9)$$

This effectively makes γ a Lagrange multiplier in a system where we specify a “target” value for the azimuthal flux, designated F_t . The additional condition (9) then forces a solution with whatever value of γ will give F_ϕ the value F_t . Therefore, we can specify all four parameters α , L^* , β , and F_ϕ (equivalently, F_t) with the hope of finding a solution.

We solve the system consisting of the discretized partial differential equation (4) and the constraint (9) using the finite-element package COMSOL MULTIPHYSICS accessed with MATLAB code; the actual solution is done with COMSOL’s nonlinear solver FEMNLIN. Before coding, we recast equation (4) in terms of the independent variable $w = 1/r$. That makes the infinite domain from $r = 1$ (solar surface) to $r = \infty$ a rectangle bounded by $w = 1$ (solar surface), $w = 0$ ($r = \infty$), $\mu = 0$ (the equatorial plane), and $\mu = 1$ (the polar axis). Since our boundary condition at the coronal base is symmetric about the equator, we need to solve in only one solar hemisphere. A uniform mesh in our rectangular w - μ domain would be nonuniform in r , giving the desired clustering of mesh points closer to the solar surface, with larger mesh elements farther out. Thus, we would have an appropriate mesh for the entire infinite domain, without having to introduce an artificial cutoff associated with an outer boundary at finite radius. However, we do not use a completely uniform mesh, but rather introduce additional mesh elements in the general region where we expect nonpotential fields. Although the gradients in the solution ψ are not unusual in the presence of electric currents, there are rapid spatial variations in the nonlinear term on the right-hand

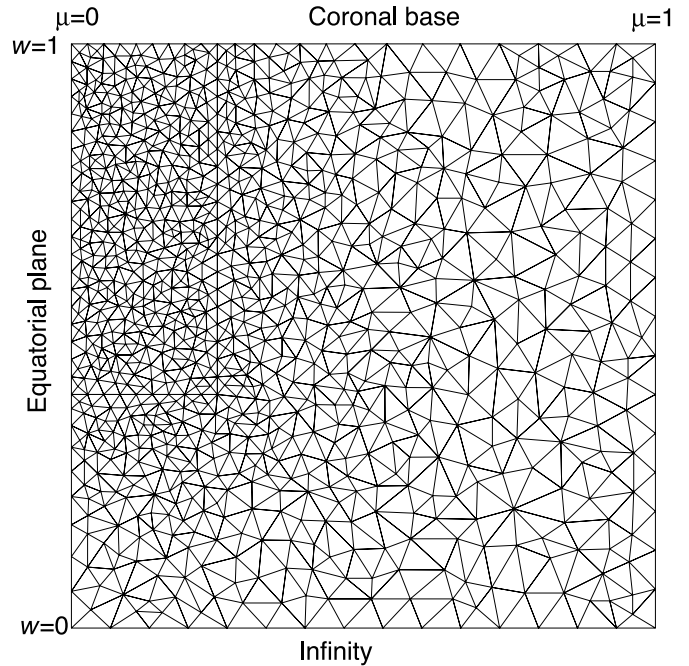


FIG. 1.— Typical finite-element mesh, but with fewer elements than used in calculations. The rectangular region at top left contains most of the nonpotential field, and here the mesh has higher resolution. The w - μ coordinate system maps the infinite computational domain into a square.

side of equation (4) at high values of γ or F_ϕ , and a fine mesh ensures that these variations are resolved. Figure 1 shows a typical mesh, although with fewer elements than we use in calculations.

5. ROLE OF THE CONFINING LATITUDE

One main goal of this work is to find out whether increased coronal magnetic energy storage results from confining the region containing electric currents with an overlying potential magnetic field. That is the purpose of our parameter L^* , which describes the latitudinal extent of nonpotential fields at the coronal base. In this section we explore the role of latitudinal confinement for the case $\alpha = 2$, representing the boundary conditions of a pure dipole. Although we will soon show that this case does not yield the greatest magnetic energy, we explore it in detail because it compares readily with FL04’s previous work on this problem. FL04 consider the cases $n = 5, 7$, and 9 , corresponding to our β taking the values $3, 4$, and 5 with no latitudinal cutoff (e.g., $L^* = 90^\circ$). They find that the maximum azimuthal flux in all three cases is about 1.7 , and that the maximum possible energy increases with n . Furthermore, their $n = 7$ and 9 solutions exhibit magnetic flux ropes. For comparison with FL04, we have explored the case $\beta = 3$, corresponding to their $n = 5$. We follow solution sequences by increasing the parameter F_ϕ as described above. Those sequences can be represented by curves in the energy versus γ plane. With a finite number of solutions calculated in each sequence, those curves become sets of discrete points. In advancing the value of F_ϕ , we use an adaptive step size adjustment that keeps the change in angle of the segment joining one pair of solution points to the segment joining the next pair in the range of 2.5° – 5° . As a result, we take smaller steps where the solution-sequence curves bend sharply. The resulting curves are similar to those on the left-hand side of Figure 2. Despite the very different computational approaches, our results for $L^* = 90^\circ$ (the unconfined case) are essentially identical to those of FL04, although we find a slight disagreement in the final few points along the

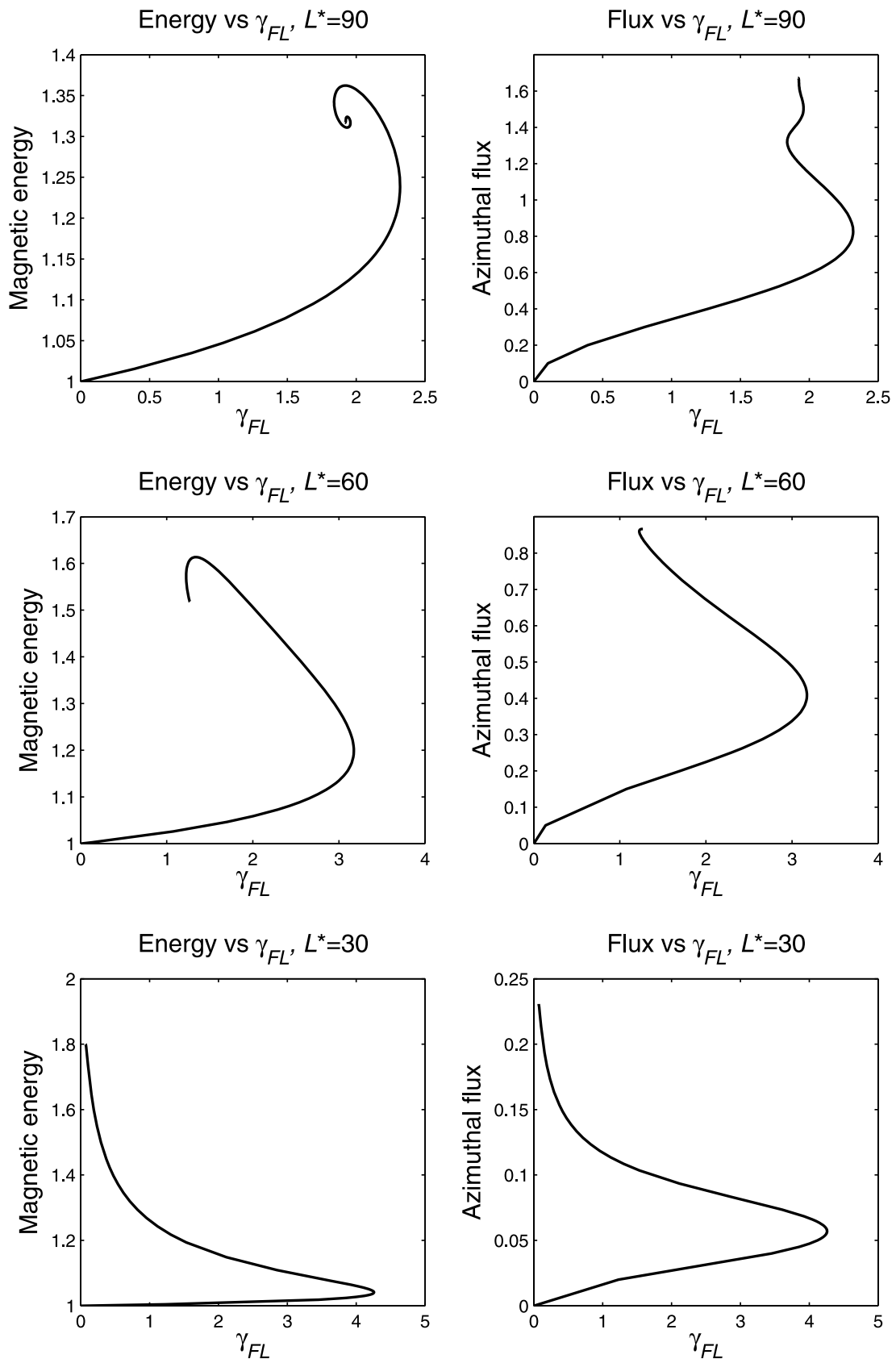


FIG. 2.—Energy and flux vs. the parameter γ_{FL} for $L^* = 90^\circ$, 60° , and 30° .

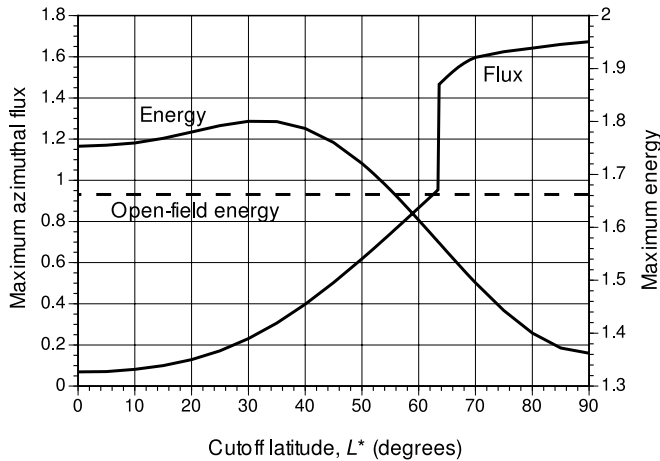


FIG. 3.—Maximum azimuthal flux and maximum magnetic energy as functions of the confining latitude L^* , for solutions with $\alpha = 2, \beta = 3$. Maximum flux and energy do not necessarily occur at the same solution, but for lower latitudes they do. The dashed line represents the energy U_{open} of the fully open field with dipole boundary conditions. Discontinuity in the flux curve marks the emergence of flux ropes from the coronal base. The dimensionless units are described in the text.

solution curve, well past the maximum energy and near what appears to be a limit point. These discrepancies probably result from the different ways in which we handle the outer boundary. More interesting is what happens as we lower the confining latitude L^* . Figure 2 shows curves of energy and flux versus the parameter γ_{FL} for $L^* = 90^\circ, 60^\circ$, and 30° . As the confining latitude decreases, so does the maximum azimuthal flux—not surprising, given that the nonpotential fields that produce this flux are now spatially limited. But even as the maximum azimuthal flux decreases, the stored magnetic energy increases. Figure 3 shows this effect for the entire latitude range. In this case the energy exhibits a slight maximum at L^* around 30° before leveling off at lower L^* values. With higher values of α , this maximum does not appear and the energy levels off at its maximum value as L^* tends toward zero (Larson 2006). In addition to this increase in magnetic energy, the confined fields develop magnetic flux ropes emerging from the coronal base—ropes that are not present for $n = 5$ in FL04’s work, when the confining latitude falls below about 64° . The discontinuity in the flux curve of Figure 3 appears to be a real feature and is associated with the appearance of these flux ropes.

Figure 3 also shows the well-known result for the energy U_{open} of the fully open field with the same dipole boundary conditions, namely 1.662 times the potential-field energy. For cutoff latitudes below about 55° , the total magnetic energy in these fields exceeds U_{open} —showing that the higher energy flux rope fields exceed the Aly-Sturrock limit on force-free fields with simpler topology. Here the greatest excess energy, while not large, is a significant 14% of the potential-field energy.

6. MAXIMIZING THE MAGNETIC ENERGY

Our primary goal is to maximize the energy of force-free fields relative to the energy of the potential field with the same boundary conditions at the coronal base. We could start with a potential-field solution and vary parameters to find higher energy solutions. However, having first done some manual exploration of parameter space, we start from a solution that already has significant energy; here we use the solution with $\alpha = 2$ (dipole boundary condition), $L^* = 20^\circ, \beta = 2$, and $F_\phi = 0.4$. This solution has 1.81 times the potential-field energy and already exceeds

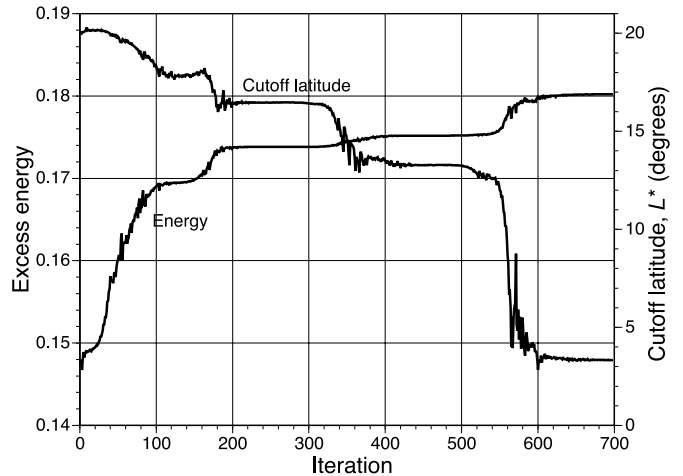


FIG. 4.—Results from the procedure that seeks the maximum-energy solution. The excess energy over that of the fully open field increases to about 18% of the potential-field energy, while the cutoff latitude drops to small values.

the open-field energy (1.662 times the potential-field energy) by almost 15% of the potential-field energy.

We then use a nonlinear maximizing routine (MATLAB’s FMINSEARCH) to find the parameter set that gives the greatest excess energy, normalized as usual to the potential-field energy for the particular value of the now-varying flux distribution parameter α . The maximizing routine takes only small steps in parameter space, so its starting point is always a nearby solution, and therefore convergence is rarely a problem. When it is a problem, we avoid that particular direction in parameter space, which means that our maximum-energy solution is only guaranteed to be the maximum among converged solutions that our procedure can reach. We also reject solutions in which the volume and surface integrals for the energy differ by more than 1 part in 10^3 , on the assumption that the solution is not sufficiently force free. In practice nearly all our solutions show agreement to about 1 part in 10^5 . Finally, we avoid directions in parameter space in which the excess energy drops by more than 10% in one step, on the grounds that the optimizing routine may have jumped to a new branch of the solution sequence.

7. MAXIMUM-ENERGY SOLUTIONS

Figure 4 shows the results of our maximum-finding procedure, along with the evolution of the cutoff latitude parameter L^* . After hundreds of iterations, the procedure converges on a maximum with parameter values $\alpha = 2.54, \beta = 0.755, L^* = 3.34$, and $F_\phi = 0.579$; Figure 5 shows the actual maximum-energy solution. At this solution the excess energy over that of the open field is just above 18% of the potential-field energy for this value of α . Figure 6 shows that this energy maximum occurs in a broad, nearly flat region in parameter space where the maximum energies exceed 17% of the potential-field energy for a wide range of parameters. Thus, our maximum-energy solution is typical of neighboring solutions. As Figure 6 implies, solutions in this high-excess-energy region show both low confining latitudes and low values of β . These trends make sense: low values of L^* mean more overlying potential field to hold down the sheared field, and low values of β spread current more broadly over the nonpotential region, resulting in higher energy associated with the azimuthal field component. It is also interesting to note that the maximum energies are reached for values of the flux distribution parameter α somewhat above the dipole value $\alpha = 2$. Since larger values of α have more flux emerging at high latitudes, this result is

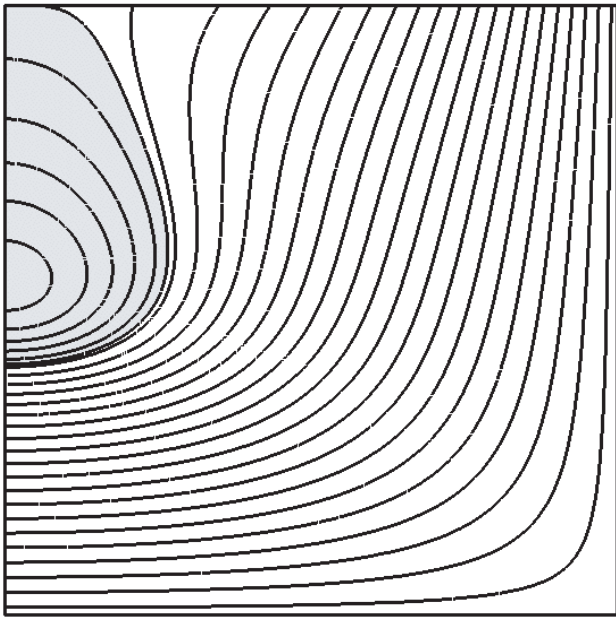


FIG. 5a

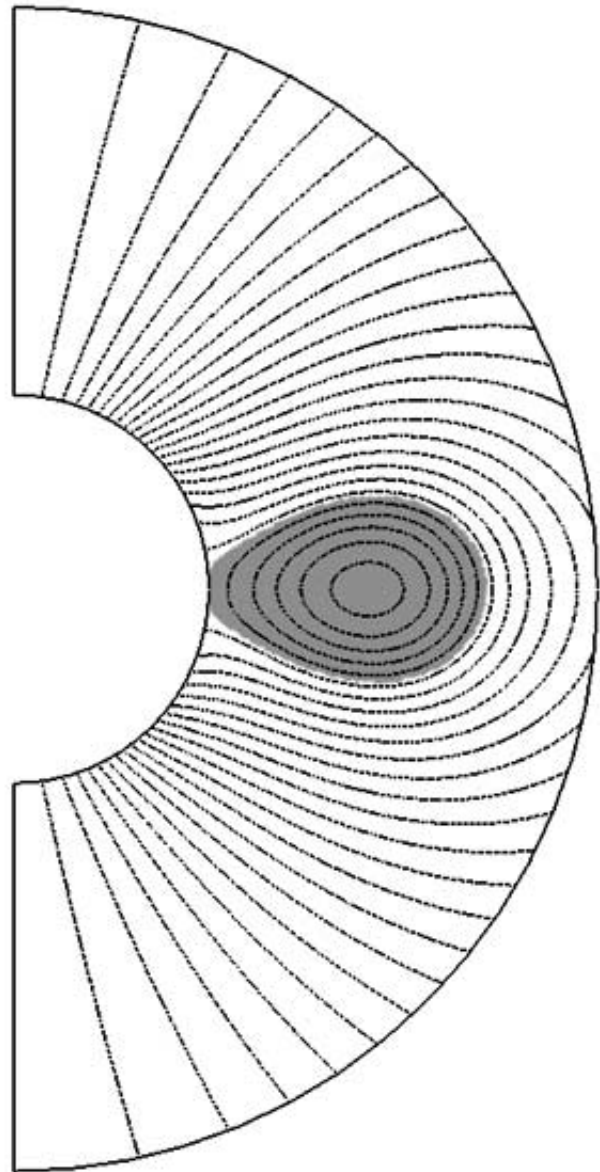


FIG. 5b

FIG. 5.—(a) Maximum-energy solution plotted on the w - μ coordinate system shown in Fig. 1. Shaded region is where the field is nonpotential. Lines are contours of the solution ψ , and represent the projection of the magnetic field lines onto the poloidal plane. Coronal base is at the top; see Fig. 1. (b) The same solution, now plotted in the usual r - θ spherical coordinates over the range $r = 1$ to 3, and mirrored into the southern hemisphere.

consistent with our finding that stronger overlying potential fields help hold down the nonpotential field, allowing larger energy buildup. We have performed additional manual and automated searches of our parameter space, including using models with higher mesh resolution, but we find no solutions with excess energies significantly different from those shown in Figures 4–6. Finer meshes do result in converged solutions for lower latitudes, but as a look at the low-latitude region of Figure 3 suggests, these are unlikely to produce significant energy gains.

8. STABILITY

Our high-energy flux rope solutions are clearly at most metastable, in the sense that there exist lower energy states to which the magnetic field might transition. The potential field is obviously one of these, but it is not relevant to the mass ejection phenomenon because CMEs leave the affected field largely open to interplan-

etary space. However, the open-field state is an obvious lower energy state that could represent the final state of an energy-decreasing field reconfiguration associated with a mass ejection. Again, our excess energies measure the difference between flux rope solutions and the open-field state. Whether there is an obvious mechanism for triggering such a reconfiguration depends on the stability of the flux rope solutions.

Our numerical equilibrium models do not readily admit stability analysis. Instead, we have used these models as inputs to the SAIC MHD code. This code solves the full resistive and viscous MHD equations on a structured grid in spherical coordinates (Mikić et al. 1999). The mesh used in the simulations was designed to have the same resolution as that of our numerical equilibrium models.

The SAIC code uses staggered grids, so we first interpolate our solutions as appropriate to the staggered grid. We also convert

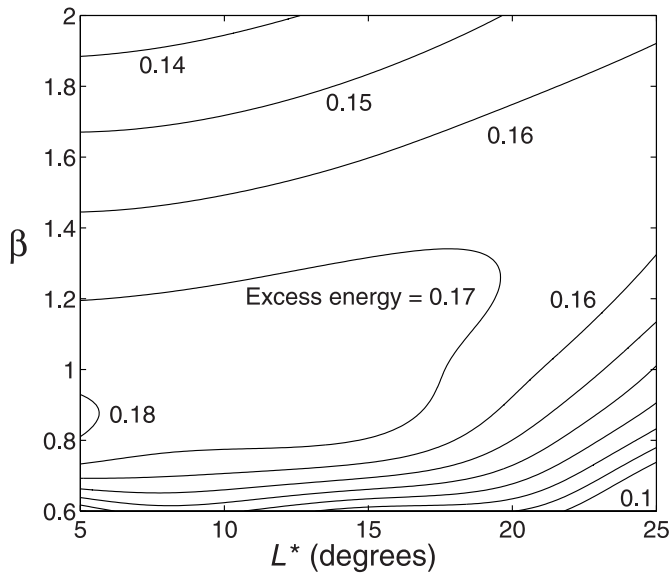


FIG. 6.—Contours of excess energy in the L^* - β plane. These were produced by interpolation on a grid of solutions spaced 0.2 in β and 5° in L^* . The maximum of Fig. 4 is off the plot to the left, within the $U_{\text{excess}} = 0.18$ contour. The flux distribution parameter α was held fixed at 2.54, its value at the true maximum, so the energies contoured do not necessarily represent the absolute maxima attainable at the different (L^*, β) values.

the flux function that is our numerical solution into the azimuthal component A_ϕ of the vector potential, as required in the SAIC code. Finally, we numerically integrate $B_\phi = f(\psi)/r \sin \theta$ in the radial direction to get the component A_θ for input to the code.

We have used our maximum-energy solutions as inputs to the SAIC code, as well as solutions with energies on either side of the open-field energy. In no case do we find any evidence of instability, at least against two-dimensional perturbations.

9. CONCLUSIONS

This work shows that detached magnetic flux ropes in the solar corona are capable of storing significantly more energy than is in

the corresponding open-field state. “Significant” here is about 18%; substantially more than the few percent found in earlier studies involving magnetic flux ropes, although somewhat less than in the more complex field geometry of Choe & Cheng (2002). Furthermore, our work suggests that a physical explanation for this energy storage is the holding down of highly sheared magnetic fields by overlying potential fields. Varying our confining latitude parameter L^* and our flux distribution parameter α shows that the highest energy solutions arise with low confining latitudes, where only a small fraction of the flux is sheared—that is, nonpotential—at the coronal base. The result is nevertheless a large nonpotential region within the coronal volume, surrounding a flux rope. Overlying this is a potential field, which if its high-latitude flux is increased, enhances the buildup of energy in the flux rope and surrounding field. So both the confinement of sheared flux at the coronal base to equatorial latitudes and the redistribution of mostly potential flux toward higher latitudes contribute to enhanced energy storage. This suggests that precursor regions for CMEs might best be found where highly nonpotential magnetic fields are confined to limited regions by strong overlying potential fields. However, our work has not found any two-dimensional instability whereby such confined, high-energy fields would spontaneously transition to the lower energy open-field state.

This work was supported primarily by NASA grant NNG04GB91G to Middlebury College. R. L. was supported by NASA’s Supporting Research and Technology and Sun-Earth Connection Theory contracts to SAIC and by NSF through the Center for Integrated Space Weather Modeling. R. W. thanks the technical support staff of COMSOL, Inc., with special thanks to COMSOL’s Nils Malm for suggesting the Lagrange-multiplier approach to our solution sequences, Rick James of Middlebury College’s Library and Information Services for help with computing setups, and Rahber Thariani of the University of Washington for recommending the use of COMSOL software in solar physics.

REFERENCES

- Aly, J. J. 1984, *ApJ*, 283, 349
 ———. 1991, *ApJ*, 375, L61
 Choe, G. S., & Cheng, C. Z. 2002, *ApJ*, 574, L179
 Flyer, N., Fornberg, B., Thomas, S., & Low, B. C. 2004, *ApJ*, 606, 1210 (FL04)
 Klimchuk, J. A., & Sturrock, P. A. 1989, *ApJ*, 345, 1034
 Larson, J. 2006, Undergraduate thesis, Middlebury College
 Li, G.-Q., & Hu, Y.-Q. 2003, *Chinese J. Astron. Astrophys.*, 3, 555
 Low, B. C. 1977, *ApJ*, 212, 234
 Mikić, Z., Linker, J. A., Schnack, D. D., Lionello, R., & Tarditi, A. 1999, *Phys. Plasmas*, 6, 2217
 Priest, E. R. 1984, *Solar Magneto-hydrodynamics* (Dordrecht: Kluwer)
 Sturrock, P. A. 1991, *ApJ*, 380, 655
 Wolfson, R. 1995, *ApJ*, 443, 810
 ———. 2003, *ApJ*, 593, 1208
 Wolfson, R., & Low, B. C. 1992, *ApJ*, 391, 353